Proceedings of the 1994 International Conference on Intelligent Robots and Systems, Munich, Germany, September 12-16, 1994

Dynamics & Control of Multi-arm Space Robots During Chase & Capture Operations

Evangelos Papadopoulos, S. Ali A. Moosavian

Department of Mechanical Engineering & Centre for Intelligent Machines
McGill University
Montreal, PQ, Canada H3A 2A7

ABSTRACT

This paper studies the motion control of a multi-arm free-flying space robot chasing a passive object in close proximity. Free-flyer kinematics are developed using a minimum set of body-fixed barycentric vectors. Using a general and a quasi-coordinate Lagrangian formulation, two dynamics models are derived. Control algorithms are developed that allow coordinated tracking control of the manipulators and the spacecraft. The performance of model-based algorithms is compared, by simulation, to that of a transposed Jacobian algorithm. Results show that the latter can give reasonably good performance with reduced computational burden.

I. INTRODUCTION

As space commercialization materializes, space structures and satellites will proliferate. Extending the life of such space systems, and therefore reducing the associated costs, will require extensive inspection, assembly and maintenance capabilities in orbit. Astronaut Extra Vehicular Activities (EVA) can be valuable in meeting these requirements. However, the cost of human life support facilities, the limited time available for astronaut EVA, and the high risks involved, make space robotic devices candidate astronaut assistants or alternatives. To increase the mobility of such devices, free-flying space robotic systems in which manipulators are mounted on a thruster-equipped spacecraft, have been proposed [1-3].

Control schemes that allow the spacecraft to be uncontrolled (free-floating mode operation), have been studied to eliminate the use of reaction jet fuel [4-8]. Control schemes for the capture of targets within a free-floating system's workspace were presented in [9,10]. However, the workspace of free-floating systems is restricted by their inability to have their system Center of Mass (CM) translated, and by the existence of workspace dynamic singularities [11]. To achieve an unlimited workspace, a control scheme that treats a free-flyer as a redundant manipulator, and is based on a pseudo-inverse Jacobian controller has been proposed [12]. In this scheme, an operator will command the manipulator's end-effector only; the spacecraft position and orientation, and the manipulator configuration will change in an uncontrolled way. In another study, a coordinated controller was designed so that both the end-effector and the spacecraft can be controlled [13]. This control scheme allows commanding a desirable manipulator configuration, and planning of a system's motions.

In this paper, the dynamics of multi-manipulator free-flying space robots are developed. The system CM position is used to represent the translational Degrees-of-Freedom (DOF). The kinematic and dynamic quantities are expressed using a set of body-fixed barycentric vectors. Next, a transposed Jacobian and two model-based motion control algorithms are designed. These algorithms permit control of both the spacecraft and its appendages in their task space. Trajectories that lead to capture of moving objects in space are planned in the spacecraft frame of reference. These trajectories take into account the relative target motion, and thruster/actuator saturation limits. The control laws are evaluated using a two manipulator free-flyer example. It is found that the model-based controllers provide good tracking, but they are computationally expensive. On the other hand, the simple Jacobian-based algorithm, when used with appropriate gains, provides an acceptable and computationally inexpensive controller.

II. DYNAMICS MODELLING

In this section, the equations of motion of a rigid multiple arm free-flying space robotic system, are obtained. The travel of the system is of relatively short length and duration and therefore the dynamical effects due to orbital mechanics are neglected. The motion of the system CM is used to describe its translation with respect to an in-orbit inertial frame of reference (XYZ), and all the kinematic and dynamic quantities are written in terms of a set of body-fixed barycentric vectors. The body 0 in Fig. 1 represents the spacecraft of the free-flyer, which is connected to n manipulators or appendages, each with N_m links. Manipulator joints are revolute and have a single DOF. The joint angles and rates are represented by N×1 column vectors $\boldsymbol{\theta}$, and $\dot{\boldsymbol{\theta}}$. The total DOF of the system are $N = K + 6$, where $K = \sum_{m=1}^{n} N_m$.

The inertial position of a point P, $\mathbf{R}_P$, can be written as

$$\mathbf{R}_P = \mathbf{R}_{CM} + \mathbf{r}_P \tag{1}$$

$$\mathbf{r}_P = \mathbf{r}_{C_i} + \mathbf{r}_{P/C_i} \tag{2}$$

where $\mathbf{r}_p$ is the position vector of P with respect to the system CM, $\mathbf{R}_{CM}$ is the inertial position of the system

CM, C_i is the CM of the i-th body, and $\mathbf{r}_{C_i}$ is its position vector with respect to the system CM. As shown in [14], $\mathbf{r}_{C_i}$ can be expressed as follows

$$\mathbf{r}_{C_0} = \tilde{\mathbf{e}}_0 + \sum_{m=1}^{n} \sum_{k=1}^{N_m} \tilde{\mathbf{l}}_k^{(m)} \tag{3}$$

$$\mathbf{r}_{C_i}^{(m)} = \tilde{\mathbf{r}}_0^{(m)} + \sum_{\substack{j=1 \\ j\neq m}}^{n} \sum_{k=1}^{N_j} \tilde{\mathbf{l}}_k^{(j)} + \sum_{k=1}^{N_m} \mathbf{v}_{ki}^{(m)} \qquad \begin{cases} m = 1,\ldots,n \\ i = 1,\ldots,N_m \end{cases} \tag{4}$$

where the superscript "m" corresponds to the m-th manipulator, the subscript "i" refers to the i-th body of that manipulator, and ($\tilde{}$) denotes body-fixed barycentric vectors defined in Appendix A.

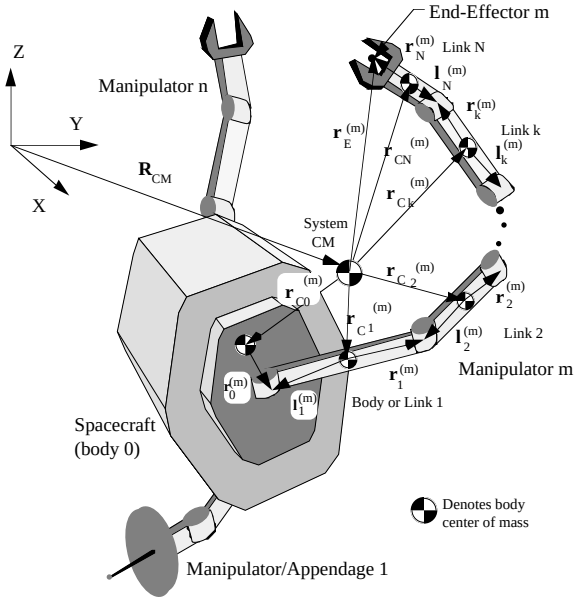

Figure 1. A free-flying space robotic system with n manipulators.

To obtain the inertial velocity of point P, Eq. (1) is differentiated and yields

$$\dot{\mathbf{R}}_p = \dot{\mathbf{R}}_{CM} + \dot{\mathbf{r}}_{C_i} + \boldsymbol{\omega}_i \times \mathbf{r}_{P/C_i} \tag{5}$$

Differentiation of Eqs. (3) and (4) yields

$$\dot{\mathbf{r}}_{C_0} = \boldsymbol{\omega}_0 \times \tilde{\mathbf{e}}_0 + \sum_{m=1}^{n} \sum_{k=1}^{N_m} \boldsymbol{\omega}_k^{(m)} \times \tilde{\mathbf{l}}_k^{(m)} \tag{6a}$$

$$\dot{\mathbf{r}}_{C_i}^{(m)} = \boldsymbol{\omega}_0 \times \tilde{\mathbf{r}}_0^{(m)} + \sum_{\substack{j=1 \\ j\neq m}}^{n} \sum_{k=1}^{N_j} \boldsymbol{\omega}_k^{(j)} \times \tilde{\mathbf{l}}_k^{(j)} + \sum_{k=1}^{N_m} \boldsymbol{\omega}_k^{(m)} \times \mathbf{v}_{ki}^{(m)} \qquad \begin{cases} m = 1,\ldots,n \\ i = 1,\ldots,N_m \end{cases} \tag{6b}$$

where $\boldsymbol{\omega}$'s are angular velocities of individual bodies, which for single DOF joints are written as

$$\boldsymbol{\omega}_i^{(m)} = \boldsymbol{\omega}_0 + \sum_{k=1}^{i} \dot{\boldsymbol{\theta}}_k^{(m)} \mathbf{z}_k^{(m)} \qquad \begin{cases} m = 1,\ldots,n \\ i = 1,\ldots,N_m \end{cases} \tag{7}$$

$\mathbf{z}_k^{(m)}$ is the unit vector along axis of rotation of the k-th joint of the m-th manipulator, and $\boldsymbol{\theta}_k^{(m)}$ is the corresponding joint angle. To obtain scalar equations, appropriate transformation matrices for each term must be employed.

The kinetic energy of the system, T, is found using Eqs. (5-7) as

$$T = \int_M \dot{\mathbf{R}}_P \cdot \dot{\mathbf{R}}_P \, dM = T_0 + T_1 \tag{8a}$$

with

$$T_0 = \frac{1}{2} M \left(\dot{\mathbf{R}}_{CM} \cdot \dot{\mathbf{R}}_{CM} \right) \tag{8b}$$

$$T_1 = \frac{1}{2} \{ m_0 \, \dot{\mathbf{r}}_{C_0} \cdot \dot{\mathbf{r}}_{C_0} + \boldsymbol{\omega}_0 \cdot \mathbf{I}_0 \cdot \boldsymbol{\omega}_0 + \sum_{m=1}^{n} \sum_{i=1}^{N_m} (m_i^{(m)} \, \dot{\mathbf{r}}_{C_i}^{(m)} \cdot \dot{\mathbf{r}}_{C_i}^{(m)} + \boldsymbol{\omega}_i^{(m)} \cdot \mathbf{I}_i^{(m)} \cdot \boldsymbol{\omega}_i^{(m)}) \} \tag{8c}$$

where $\mathbf{I}_i^{(m)}$ is the inertia dyadic of the i-th body of the m-th manipulator with respect to its CM. Using Eqs. (6-8), the kinetic energy of the system can be written as

$$T = \frac{1}{2} \mathbf{v}^T \mathbf{H}(\boldsymbol{\theta}) \mathbf{v} \tag{9}$$

where $\mathbf{v} = (\dot{\mathbf{R}}_{CM}^T, {}^0\boldsymbol{\omega}_0{}^T, \dot{\boldsymbol{\theta}}^T)^T$ is the vector of generalized velocities, and the matrix $\mathbf{H}$ is an N×N positive definite mass matrix. The vector ${}^0\boldsymbol{\omega}_0$ is the spacecraft angular velocity expressed in its frame of reference. For the free-flyer, the microgravity effects compared to control forces are very small and hence they are neglected; the system potential energy is taken equal to zero. Using the expression for the kinetic energy given by Eq. (9), and a quasi-Lagrangian approach [15], a set of dynamical equations is obtained in the form

$$\mathbf{H}(\boldsymbol{\theta}) \dot{\mathbf{v}} + \mathbf{C}({}^0\boldsymbol{\omega}_0, \boldsymbol{\theta}, \dot{\boldsymbol{\theta}}) = \mathbf{Q} \tag{10}$$

where C contains all the nonlinear velocity terms, and Q is the vector of generalized forces given by

$$\mathbf{Q} = \begin{Bmatrix} \mathbf{0}_{6\times 1} \\ \boldsymbol{\tau}_{K\times 1} \end{Bmatrix} + \sum_{i=0}^{N} \sum_{p=1}^{i_f} \mathbf{J}_{i,p}{}^T \mathbf{F}_{i,p} \tag{11}$$

The vector $\boldsymbol{\tau}$ contains joint torques, $\mathbf{F}_{i,p}$ is the p-th external force/moment applied on the i-th body, i_f is the number of applied forces/moments on the i-th body, and $\mathbf{J}_{i,p}$ is a Jacobian matrix corresponding to the point of force/moment application. Eq. (11) can be rearranged, so that actuator forces/torques are displayed explicitly. If other external forces are zero, $\mathbf{Q}$ can be written as

$$\mathbf{Q} = \mathbf{J}_Q{}^T \begin{Bmatrix} {}^0\mathbf{f}_s \\ {}^0\mathbf{n}_s \\ \boldsymbol{\tau}_{K\times 1} \end{Bmatrix} \tag{12}$$

where ${}^0\mathbf{f}_s$ and ${}^0\mathbf{n}_s$ are the net force and moment applied to the spacecraft, and $\mathbf{J}_Q$ is an N×N Jacobian matrix. For a well designed system, $\mathbf{J}_Q$ is nonsingular, that is any required $\mathbf{Q}$ vector can be produced by the system's actuators.

The form of equations in (10) is useful in designing an Euler-parameter based control algorithm, as discussed in more detail in Section III. For control reasons, it is also beneficial to obtain the equations of motion using as the vector of generalized coordinates $\mathbf{q} = (\mathbf{R}_{CM}^T, \boldsymbol{\delta}^T, \boldsymbol{\theta}^T)^T$, where $\boldsymbol{\delta}$ is a set of Euler angles that describe the orientation of the spacecraft. The spacecraft angular velocity can be expressed in terms of the Euler rates as [15]

$$ {}^0\boldsymbol{\omega}_0 = \mathbf{S}_0(\boldsymbol{\delta})\,\dot{\boldsymbol{\delta}} \tag{13} $$

where $\mathbf{S}_0(\boldsymbol{\delta})$ is a 3×3 matrix, function of the attitude $\boldsymbol{\delta}$ Then the kinetic energy can be written as

$$ T = \frac{1}{2}\,\dot{\mathbf{q}}^T \mathbf{H}_{\boldsymbol{\delta}}(\boldsymbol{\delta}, \boldsymbol{\theta})\dot{\mathbf{q}} \tag{14} $$

Applying Lagrange's equations to Eq. (14)

$$ \frac{d}{dt}\left(\frac{\partial T}{\partial \dot{q}_i}\right) - \left(\frac{\partial T}{\partial q_i}\right) = Q_{\boldsymbol{\delta},i} \qquad i = 1, \ldots, N \tag{15} $$

results in the dynamics model of the system

$$ \mathbf{H}_{\boldsymbol{\delta}}(\boldsymbol{\delta}, \boldsymbol{\theta})\,\ddot{\mathbf{q}} + \mathbf{C}_{\boldsymbol{\delta}}(\boldsymbol{\delta}, \dot{\boldsymbol{\delta}}, \boldsymbol{\theta}, \dot{\boldsymbol{\theta}}) = \mathbf{Q}_{\boldsymbol{\delta}} \tag{16} $$

The vector $\mathbf{Q}_{\boldsymbol{\delta}}$ is related to $\mathbf{Q}$ by a simple transformation. The equations of motion derived in this section will be used in designing control algorithms, the topic of the next section.

III. CONTROL DESIGN

Controlling a free-flyer space robot requires definition of the controlled system outputs, and design of a control law which can guarantee that these outputs will track asymptotically desired trajectories. A designer is faced with many options for the controlled outputs. These include joint space variables, Cartesian (task) space variables, and others. The various orientation representations further increase the available options. In this paper, the focus is in controlling the Cartesian position/orientation of the spacecraft and the endpoints of its appendages (manipulators). End-effector orientations are described either by Euler angles or by Euler parameters.

1. Model-based Control Design Using Euler Angles (MB1)

Step 1. Transform the equations of motion (16) in terms of the output coordinates $\hat{\mathbf{q}}$ given by

$$ \hat{\mathbf{q}} = [\mathbf{R}_0^T, \boldsymbol{\delta}^T, \mathbf{x}_E^{(1)T}, \boldsymbol{\delta}_E^{(1)T}, \ldots, \mathbf{x}_E^{(n)T}, \boldsymbol{\delta}_E^{(n)T}]^T \tag{17} $$

where $\mathbf{x}_E^{(m)}$ and $\boldsymbol{\delta}_E^{(m)}$ correspond to the m-th end-effector position and orientation. If all manipulators have six DOF, then a system of n manipulators will have 6n+6 DOF, and $\hat{\mathbf{q}}$ will be a 6n+6 vector. The output velocities $\dot{\hat{\mathbf{q}}}$ are obtained from the generalized velocities $\dot{\mathbf{q}}$ using a square Jacobian $\mathbf{J}_{\hat{q}}$

$$ \dot{\hat{\mathbf{q}}} = \mathbf{J}_{\hat{q}}(\boldsymbol{\delta}, \boldsymbol{\theta})\,\dot{\mathbf{q}} \tag{18} $$

The Jacobian $\mathbf{J}_{\hat{q}}$ is not singular, except when a manipulator is at a singular configuration, or at a (non-physical) representation singularity due to the use of Euler angles. The latter can be avoided by switching to a different set of Euler angles. The equations of motion are then

$$ \hat{\mathbf{H}}_{\delta}\,\ddot{\hat{\mathbf{q}}} + \hat{\mathbf{C}}_{\delta} = \mathbf{J}_{\hat{q}}^{-T}\,\mathbf{Q}_{\delta} \tag{19} $$

where $\hat{\mathbf{C}}_{\delta}$ contains the nonlinear terms, and $\hat{\mathbf{H}}_{\delta}$ is given by

$$ \hat{\mathbf{H}}_{\delta} = \mathbf{J}_{\hat{q}}^{-T}\,\mathbf{H}_{\delta}\,\mathbf{J}_{\hat{q}}^{-1} \tag{20} $$

This inertia matrix is positive definite if $\mathbf{J}_{\hat{q}}$ is nonsingular.

Step 2. Use the model-based control law

$$ \mathbf{Q}_{\delta} = \mathbf{J}_{\hat{q}}^T\,\{\hat{\mathbf{H}}_{\delta}\,\mathbf{u} + \hat{\mathbf{C}}_{\delta}\} \tag{21} $$

where it is assumed that the system geometric and mass properties are known, and where $\mathbf{u} = [\mathbf{u}_{\mathbf{R}}{}^T, \mathbf{u}_{\boldsymbol{\delta}}{}^T, \mathbf{u}_{\mathbf{x}}^{(1)T}, \mathbf{u}_{\boldsymbol{\delta}}^{(1)T}, \ldots, \mathbf{u}_{\mathbf{x}}^{(n)T}, \mathbf{u}_{\boldsymbol{\delta}}^{(n)T}]$ is an auxiliary control signal. This control law linearizes and decouples the system equations to a set of second order differential equations

$$ \ddot{\hat{\mathbf{q}}} = \mathbf{u} \tag{22} $$

Step 3. If $\mathbf{u}$ is computed such that

$$ \mathbf{u} = \mathbf{K}_p\,\mathbf{e} + \mathbf{K}_d\,\dot{\mathbf{e}} + \ddot{\hat{\mathbf{q}}}_{des} \tag{23} $$

where $\mathbf{K}_p$, and $\mathbf{K}_d$ are positive definite diagonal matrices, and $\mathbf{e}$ is the tracking error defined as

$$ \mathbf{e} = \hat{\mathbf{q}}_{des} - \hat{\mathbf{q}} \tag{24} $$

then, the control law given by Eq. (21) guarantees asymptotic convergence of the tracking error $\mathbf{e}$. The desired trajectory, $\hat{\mathbf{q}}_{\text{des}}$, is provided by a trajectory planner, while $\hat{\mathbf{q}}$ can be obtained from inertial measurements of the position and orientation of the spacecraft and of the end-effectors. If no such measurements are available, the error $\mathbf{e}$ can be estimated by integrating the equations of motion in real time, but then errors due to model uncertainties will be introduced.

2. Transposed Jacobian Control Design (TJ)

If high enough gains are used, the simpler transposed Jacobian controller can be employed, [13,18]

$$ \mathbf{Q}_{\delta} = \mathbf{J}_{\hat{q}}^T\,\{\mathbf{K}_p\,\mathbf{e} + \mathbf{K}_d\,\dot{\mathbf{e}}\} \tag{25} $$

This algorithm is quite simple to use. Its action can be understood by imagining generalized springs and dampers connected between the bodies under control and the desired

trajectories; the stiffer the gains are, the better the tracking should be. Note that if a physical singularity is encountered, the controller given by Eq. (25) will result in errors but will not fail computationally.

3. Model-based Control using Euler Parameters (MB2)

Euler angle based control algorithms present the inconvenience of representation singularities, i.e. inversion of relations similar to Eq. (13) is not possible at some orientation. At such points, a different set of Euler angles must be used. It is expected that some singularity will appear whenever a three-parameter description of the orientation is employed. However, a great improvement can occur if the singularity appears at some *attitude error* and not at some *attitude*. An Euler parameter based control algorithm that achieves this condition has been presented for the attitude control of a rigid body, and is adapted here for the control of a free-flyer [16]. The adaptation of this algorithm requires some modification of the three steps outlined above.

Step 1. Transform the equations of motion (10) in terms of the output velocities $\hat{\mathbf{v}}$ given by

$$\hat{\mathbf{v}} = [\dot{\mathbf{R}}_0^T,\ {}^0\boldsymbol{\omega}_0^T, \dot{\mathbf{x}}_E^{(1)T},\ {}^1\boldsymbol{\omega}_E^{(1)T}, \ldots, \dot{\mathbf{x}}_E^{(n)T},\ {}^n\boldsymbol{\omega}_E^{(n)T}]^T \tag{26}$$

where $\dot{\mathbf{x}}_E^{(m)}$ and ${}^m\boldsymbol{\omega}_E^{(m)T}$ are the m-th end-effector linear and angular inertial velocity, expressed in the inertial and m-th body frame, respectively. If all manipulators have six DOF, then a system of n manipulators will have 6n+6 DOF, and $\hat{\mathbf{v}}$ will be a 6n+6 vector. The output velocities $\hat{\mathbf{v}}$ are obtained from the generalized velocities $\mathbf{v}$ by a Jacobian $\mathbf{J}_{\hat{v}}$

$$\hat{\mathbf{v}} = \mathbf{J}_{\hat{v}}(\boldsymbol{\varepsilon}, n, \boldsymbol{\theta})\mathbf{v} \tag{27}$$

where $\boldsymbol{\varepsilon}$ and n are the vector and scalar part of Euler parameters, representing the orientation of the spacecraft [17]. The equations of motion are then

$$\hat{\mathbf{H}}\dot{\hat{\mathbf{v}}} + \hat{\mathbf{C}} = \mathbf{J}_{\hat{v}}^{-T}\mathbf{Q} \tag{28}$$

where $\hat{\mathbf{C}}$ contains the nonlinear terms, and $\hat{\mathbf{H}}$ is given by

$$\hat{\mathbf{H}} = \mathbf{J}_{\hat{v}}^{-T}\mathbf{H}\,\mathbf{J}_{\hat{v}}^{-1} \tag{29}$$

Step 2. Use the model-based control law

$$\mathbf{Q} = \mathbf{J}_{\hat{v}}^{T}\{\hat{\mathbf{H}}\mathbf{u} + \hat{\mathbf{C}}\} \tag{30}$$

where $\mathbf{u}$ is an auxiliary control input, under the assumption of knowledge of a system's properties. Applying this law to the equations of motion (28) results in the following decoupled system

$$\dot{\hat{\mathbf{v}}} = \mathbf{u} \tag{31}$$

Note that Eq. (31) is expressed in terms of linear and angular velocities, and not in terms of positions and Euler angles as is the case in Eq. (22).

Step 3. Use an auxiliary control signal $\mathbf{u}$, partitioned as $\mathbf{u} = [\mathbf{u}_{\dot{\mathbf{R}}}^T, \mathbf{u}_{\boldsymbol{\omega}}^T, \mathbf{u}_{\dot{\mathbf{x}}}^{(1)T}, \mathbf{u}_{\boldsymbol{\omega}}^{(1)T}, \ldots, \mathbf{u}_{\dot{\mathbf{x}}}^{(n)T}, \mathbf{u}_{\boldsymbol{\omega}}^{(n)T}]^T$, where the partition follows that of $\hat{\mathbf{v}}$. The acceleration terms in Eq. (31) that correspond to linear motions are controlled similarly to Eq. (23). For example, $\mathbf{u}_{\dot{\mathbf{R}}}$ is given by

$$\mathbf{u}_{\dot{\mathbf{R}}} = \mathbf{K}_{p,\dot{\mathbf{R}}}\mathbf{e}_{\dot{\mathbf{R}}} + \mathbf{K}_{d,\dot{\mathbf{R}}}\dot{\mathbf{e}}_{\dot{\mathbf{R}}} + \ddot{\mathbf{R}}_{0,des} \tag{32}$$

where

$$\mathbf{e}_{\dot{\mathbf{R}}} = \mathbf{R}_{0,des} - \mathbf{R}_0 \tag{33}$$

However, the terms that correspond to angular velocities are controlled as

$$\mathbf{u}_{\omega} = \mathbf{R}_e\dot{\boldsymbol{\omega}}_{des} + \boldsymbol{\omega}^{\times}\boldsymbol{\omega}_e - \mathbf{K}_v\boldsymbol{\omega}_e - 2(\mathbf{K}_p - \boldsymbol{\omega}_e^T\boldsymbol{\omega}_e/4)\boldsymbol{\varepsilon}_e/n_e \tag{34}$$

In the above law, subscripts *e* and *des* correspond to error and desired quantities respectively. All $\boldsymbol{\omega}$'s are expressed in the corresponding body frame. Detailed expressions for computing Eq. (34) are given in Appendix B. Applying the control law given by Eq. (30) guarantees asymptotic convergence for the positional errors, and asymptotic convergence for the attitude error expressed in terms of Euler parameters. Note that due to the form of Eq. (34), singularities occur only when n_e is zero, that is when the attitude error angle is π rad about any eigen axis. This problem can be tackled by a simple modification [16].

Note that all the above algorithms employ PD action; however, integral action can be easily incorporated. Finally, the reaction jet forces and torques and the joint torques can be found by inverting an equation relating generalized forces to actuator forces, for example Eq. (12).

IV. SIMULATIONS & COMPARISONS

In this section, the control algorithms developed in Section III are compared and evaluated. To this end, a planar free-flyer chasing a moving point target, is employed. The free-flyer includes three open chain appendages, two of which are two-link manipulators, while the third is a communications antenna, see Fig. 2.

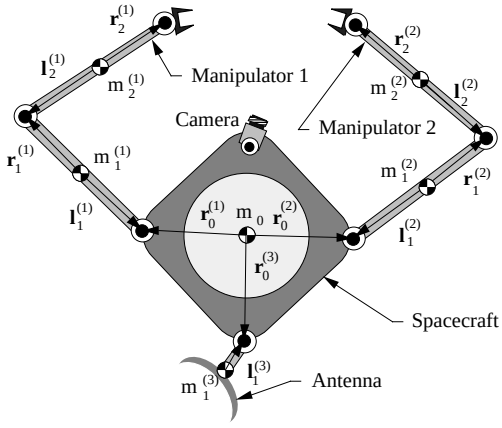

Figure 2. A planar three appendage / manipulator free-flyer.

The spacecraft is equipped with reaction jets which provide the required control forces and torques up to some limited values. The system geometric parameters and mass

properties, and the maximum available actuator forces/torques are displayed in Table I. The origin of the inertial frame coincides with the initial position of the system CM.

The vector of generalized coordinates for this 8-DOF system is

$$\mathbf{q} = [x_{CM}, y_{CM}, \theta_0, \theta_1^{(1)}, \theta_2^{(1)}, \theta_1^{(2)}, \theta_2^{(2)}, \theta_1^{(3)}]^T \qquad (35)$$

while the vector of coordinates to be controlled is

$$\hat{\mathbf{q}} = [x_0, y_0, \theta_0, x_E^{(1)}, y_E^{(1)}, x_E^{(2)}, y_E^{(2)}, \delta^{(3)}]^T \qquad (36)$$

where x_{CM} and y_{CM} are the inertial coordinates of the system CM, x_0 and y_0 are the inertial coordinates of the spacecraft CM, θ_0 is the spacecraft attitude, $\theta_i^{(j)}$ is the i-th joint angle of the j-th manipulator, and $x_E^{(i)}$, $y_E^{(i)}$, and $\delta^{(i)}$ are the inertial coordinates and attitude of the i-th end-effector.

Table I-a. Spacecraft parameters and actuator limits.

$r_0^{(1)}$ (m)	$r_0^{(2)}$ (m)	$r_0^{(3)}$ (m)	m_0 (kg)	I_0 (kg m^2)	F_x (N)	F_y (N)	τ_0 (N-m)
0.5	0.5	0.5	50.0	10.0	20.0	20.0	10.0

Table I-b. Manipulator parameters and joint actuator limits.

Appe-ndage	i-th body	$r_i^{(m)}$ (m)	$l_i^{(m)}$ (m)	$m_i^{(m)}$ (kg)	$I_i^{(m)}$ (kgm^2)	$\tau_i^{(m)}$ (N-m)
1	1	0.50	0.50	4.0	0.50	7.0
1	2	0.50	0.50	3.0	0.25	5.0
2	1	0.50	0.50	4.0	0.50	7.0
2	2	0.50	0.50	3.0	0.25	5.0
3	1	0.25	0.25	5.0	2.00	7.0

To ensure smooth operation, appropriate trajectories for the spacecraft motion are planned. It is assumed that the target is in the vicinity of the robotic system, drifting at some constant speed, and that its trajectory is measured by such feedback devices as on-board cameras. Hence, the position and velocity of the target is available in the spacecraft frame. If inertial feedback is provided to the free-flyer by external measurement devices, this can be transformed to the spacecraft's frame.

1. Trajectory Planning. To plan trajectories for the spacecraft, a motion final time, t_f, is first selected. Then, the required spacecraft position at t_f is found as follows. If ${}^0\mathbf{x}_{obj}(0)$ and ${}^0\mathbf{v}_{obj}(0)$ are the position and velocity of the object as measured from the spacecraft at initial time, then the final position of the spacecraft CM, ${}^0\mathbf{x}_f$, is given by

$${}^0\mathbf{x}_f = {}^0\mathbf{x}_{obj}(0) + [{}^0\mathbf{v}_{obj}(0) + {}^0\mathbf{v}_0]\, t_f + {}^0\mathbf{r} \qquad (37)$$

where ${}^0\mathbf{v}_0$ is the initial velocity of the spacecraft, and ${}^0\mathbf{r}$ defines the relative position of the spacecraft CM and the object at t_f. The direction of ${}^0\mathbf{r}$ is along the line connecting the spacecraft CM at initial time with the object location at t_f, and its magnitude is such that the manipulators can work on the object. During capture, it is desired to have the object stationery in the spacecraft frame, so the final spacecraft velocity, ${}^0\mathbf{v}_f$, is chosen as

$${}^0\mathbf{v}_f = {}^0\mathbf{v}_{obj}(0) + {}^0\mathbf{v}_0 \qquad (38)$$

For trajectory planning, parabolic trajectories made of constant acceleration, constant velocity, and constant deceleration segments are employed. Given ${}^0\mathbf{x}_f$, ${}^0\mathbf{v}_f$, the maximum acceleration $\mathbf{a}_1$, the maximum deceleration $\mathbf{a}_2$, and t_f, time t_1 at which the acceleration segment ends, and time t_2 at which the deceleration segment starts, can be computed. Note that the off/on times, t_1 and t_2, are not necessarily equal for the three components describing the spacecraft's position and orientation. Estimates for $\mathbf{a}_1$ and $\mathbf{a}_2$ can be obtained using thruster force capabilities and the mass properties of the system.

After computing the desired trajectory in the spacecraft frame, ${}^0\mathbf{x}(t)$, the trajectory in inertial space can be computed by

$$\mathbf{X}(t) = \mathbf{X}_0 + \mathbf{T}_0\ {}^0\mathbf{x}(t) \qquad (39)$$

where $\mathbf{T}_0$ is the transformation matrix between the spacecraft frame at initial time and the inertial frame, $\mathbf{X}_0$ is the inertial position of the spacecraft CM at initial time, and $\mathbf{X}(t)$ is the inertial trajectory. In practice, the object would be under observation during the chase phase. Should its trajectory change significantly, a new spacecraft chase trajectory could be re-planned following the same procedure.

The desired trajectory for the orientation of the spacecraft, is similarly planned. The final orientation is chosen so as to provide an approximately symmetric motion of the manipulators during capture, since this strategy can minimize spacecraft disturbances.

The manipulators remain in their home configuration as long as the final position of the object is not in their fixed-base reachable workspace. During that period, a joint-space controller acting as a brake, is used. When the object enters the reachable workspace of an end-effector, a quintic trajectory [18], is planned in the task space for that end-effector. This trajectory provides position, velocity, and acceleration continuity throughout the motion. During this phase, a task-space control algorithm is applied. For the third appendage, i.e. the communications antenna, a constant attitude is commanded throughout the maneuver.

2. Simulation Results. For the simulation results that follow, the object initial position and relative velocity was taken as ${}^0\mathbf{x}_{obj}(0) = [3.0, 4.0]^T$ m, and ${}^0\mathbf{v}_{obj}(0) = [0.05, 0.1]^T$ m/s, respectively. The initial position of the spacecraft in inertial frame was $[x_0(0), y_0(0), \theta_0(0)]^T = [-0.0485\text{m}, -.0659\text{m}, -\pi/6\text{rad}]^T$, and its inertial initial velocity $[\dot{x}_0(0), \dot{y}_0(0), \dot{\theta}_0(0)]^T = (0.01\text{m/s}, 0.01\text{m/s}, 0.001\text{rad/s}]^T$. Taking into account the mass properties of the system and the available thruster forces/torques, the maximum acceleration and deceleration was set to

$\mathbf{a}_1 = [0.2, 0.2]^T\, m/s^2$, $\mathbf{a}_2 = 0.2\mathbf{a}_1$ for the linear motion, and a_1 = 0.05 rad/s^2, $a_2 = 0.5a_1$ for the rotational motion. The initial generalized coordinates vector was $\mathbf{q}(0)$ = [0,0,-30°,-45°,90°,135°,-90°,30°]^T.

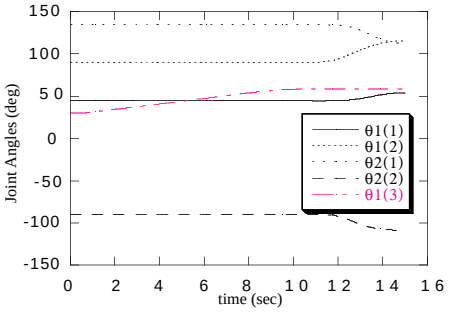

(a)

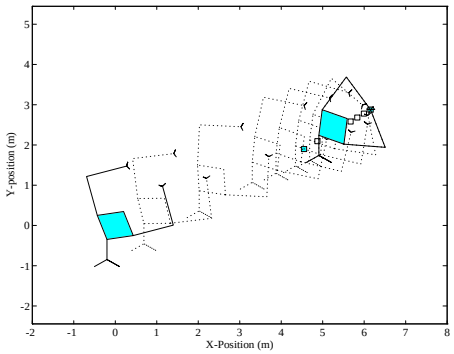

(b)

Figure 3. (a) Joint angle histories for the two manipulators and the antenna, (b) Animated view of the maneuver.

For this system, the two model-based control algorithms (MB1, MB2), yield almost identical results, and so only results corresponding to the first control law are presented here. The comparison between these two in the 3-D case is under current study. To include the effects of model uncertainties in the MB laws, the mass properties of the model used in the control algorithm were perturbed with respect to the "true" parameters by up to 30%. The gains used for the MB1 controller were $\mathbf{K}_p$ = diag(70,70,100,100, 100,100,100,70), and $\mathbf{K}_d$ = diag(15,15,15,15,15,15, 15,15), while for the TJ controller the gains were $\mathbf{K}_p$ = diag(100, 100,80,80,80,80,80,80), and $\mathbf{K}_d$ = diag(150,150,100,100, 100,100,100,100). The gain selection for the model-based control was based on error equation settling time and damping criteria, while for the TJ control a heuristic approach was used.

Fig. 3 depicts the motion of the joints during the maneuver and an animated view of it. Note that the joint angles for the two-link manipulators remain constant during the chase phase (in home configuration), and that they change smoothly during the capture phase (object in manipulator workspace). The joint angle for the third appendage, i.e. the antenna, changes smoothly so that a fixed inertial orientation is maintained during the maneuver.

Figures 4 and 5 can be used to compare and evaluate MB1 and TJ algorithms. Figures 4(a) and 5(a) display the tracking error for the first manipulator end-effector in the task space. During the chase phase, this error is almost zero, as the manipulators are kept fixed at their home positions. When the object enters the manipulator workspace, the manipulators start moving, and tracking errors appear due to dynamic coupling and to transition to the task-space control phase. These errors decrease with time and eventually vanish, in both algorithms. Comparison of the maximum values of the tracking errors for the two algorithms shows that the errors occurring with TJ are about thirty times larger than the errors with MB1. However, their absolute magnitude is small enough. Comparison of the spacecraft thruster forces, shows that the required forces are about the same for both algorithms, see Figures 4(b), and 5(b), while the required torques are lower in MB1, see Figures 4(c), and 5(c). The variation of the applied torques follows the variation of spacecraft attitude and also tracking errors, which is due to the same reasons, as above.

As shown by simulation, MB1 results in smaller errors and smaller required torques and yields better results even in the presence of model uncertainties. Since torques are lower, smaller actuators would be required, resulting in reduced system weight, an important issue in space. However, implementing a model-based control requires increased computational burden, which may not be available, while at the same time it reduces the closed-loop bandwidth. On the other hand, TJ control yields acceptable results, and can be considered as a good control algorithm candidate, especially when larger bandwidths and low computational costs are required.

V. CONCLUSIONS

In this paper, the motion control of a multi-manipulator free-flying space robot chasing a passive object in close proximity was studied. Using a minimum set of body-fixed barycentric vectors, and Lagrangian formulations based on quasi-coordinates, and on generalized coordinates, dynamic models were derived. Control algorithms are developed that allow coordinated tracking control of the manipulators and the spacecraft. These include two model-based control laws (an Euler angle, and an Euler parameter based control law), and a simpler transposed Jacobian control law. The performance of the model-based algorithms is compared by simulation to that of the transposed Jacobian algorithm. Results indicate that the latter can give reasonably good performance with reduced computational burden.

VI. ACKNOWLEDGMENTS

The support of this work by the Natural Sciences and Engineering Council of Canada (NSERC) is acknowledged. The second author would also like to acknowledge support from the Iran Ministry of Higher Education.

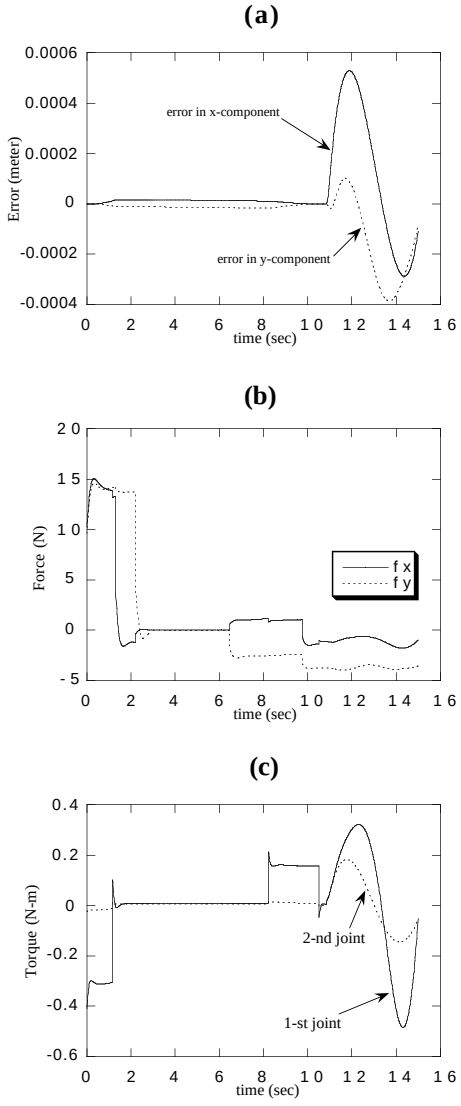

Figure 4. Model-Based Control. (a) Tracking position errors for the first end-effector, (b) Thruster forces on the spacecraft, (c) Joint torques for the first manipulator.

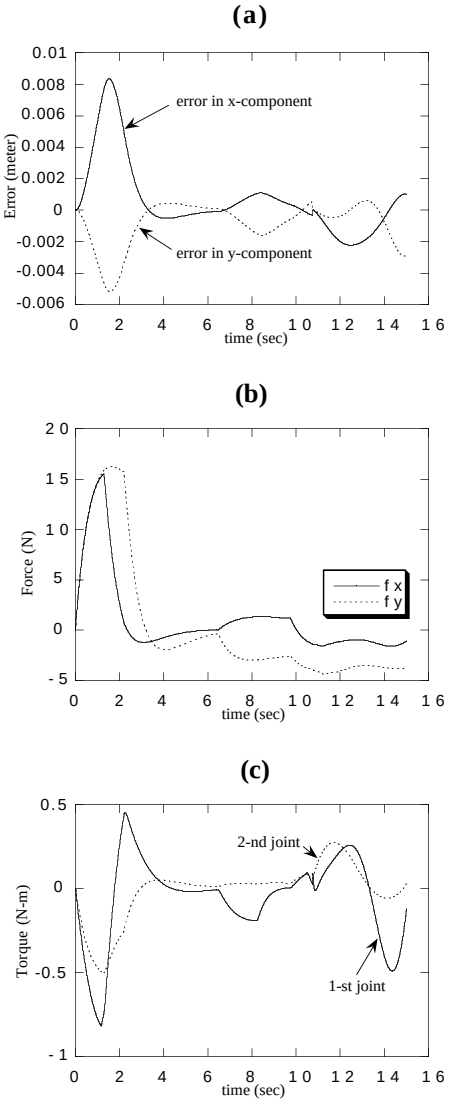

Figure 5. Jacobian Transposed Control. (a) Tracking position errors for the first end-effector, (b) Thruster forces on the spacecraft, (c) Joint torques for the first manipulator.

REFERENCES

[1] Bronez, M. A., Clarke, M. M., and Quinn A., "Requirements Development for a Free-Flying Robot - the ROBIN," in *Proc. of the IEEE International Conference on Robotics and Automation*, San Fransisco, CA, April 1986.

[2] Reuter, G. J., et al. "An Intelligent, Free-Flying Robot," in "Space Station Automation IV," Chiou, W.C. ed., *SPIE Proceedings Series*, Vol. 1006, November 1988, pp. 20-27.

[3] Space Robots R&D in Japan, Special Issue of *New Technology Japan*, JETRO, Tokyo, Japan, 1990.

[4] Alexander, H. and Cannon, R., "Experiments on the Control of a Satellite Manipulator," *Proc. 1987 American Control Conf.*, Seattle, WA, June 1987.

[5] Umetani, Y. and Yoshida, K., "Resolved Motion Control of Space Manipulators with Generalized Jacobian Matrix," *IEEE Trans. on Robotics and Automation*, Vol. 5, No. 3, 1989, pp. 303-314.

[6] Vafa, Z. and Dubowsky, S., "On the Dynamics of Space Manipulators Using the Virtual Manipulator, with Applications to Path Planning," *J. Astr. Sciences*, Vol. 38, No. 4, 1990, pp. 441-472.

[7] Masutani, Y., Miyazaki, F., and Arimoto, S., "Sensory Feedback Control for Space Manipulators," *Proc. IEEE Int. Conf. on Robotics & Automation*, Scottsdale, AZ, May 1989.

[8] Papadopoulos, E. and Dubowsky, S., "On the Nature of Control Algorithms for Free-floating Space Manipulators," *IEEE Trans. on Robotics and Automation*, Vol. 7, No. 6, Dec. 1991, pp. 750-758.

[9] Fujii, H., et al., "Capture Control for Manipulator Arm of Free-flying Space Robot," *AIAA Paper*, AIAA-90-3432-CP, 1990.

[10] Yoshida, K., "Space Structure Capturing and Assembling by Experimental Free-floating Robot Satellite (EFFORTS) Simulators," *Proc. Dynamics and Control in Space*, Cranfield, UK, Sep. 1993.

[11] Papadopoulos, E. and Dubowsky, S., "Dynamic Singularities in the Control of Free-Floating Space Manipulators," *ASME Journal of Dynamic Systems, Measurement and Control*, Vol. 115, No. 1, March 1993, pp. 44-52. Also in *Space Robotics: Dynamics and Control*, Y. Xu, and T. Kanade eds., Kluwer, Boston, MA, 1993, pp. 77-100.

[12] Spofford, J., and Akin, D., "Redundancy Control of a Free-Flying Telerobot," *Proc. of the AIAA Guidance, Navigation and Control Conference*, Minneapolis, MN, August 1988.

[13] Papadopoulos, E. and Dubowsky, S., "Coordinated Manipulator/Spacecraft Motion Control for Space Robotic Systems," *Proc. of the IEEE Int. Conf. on Robotics and Automation*, Sacramento, CA, April 1991, pp. 1696-1701.

[14] Papadopoulos, E., "Large Payload Manipulation by Space Robots," *Proc. of the Int. Conf. on Intelligent Robots and Systems*, Yokohama, Japan, July 26-30, 1993.

[15] Meirovitch, L., *Methods of Analytical Dynamics*, McGraw-Hill, 1970.

[16] Paielli, R. A. and Bach, R. E., "Attitude Control with Realization of Linear Error Dynamics," *J. of Guidance, Control, and Dynamics*, Vol. 16, No. 1, 1993, pp. 182-189.

[17] Hughes, P.C., *Spacecraft Attitude Dynamics*, John Wiley, New York, NY, 1986.

[18] Craig, J., *Introduction to Robotics, Mechanics and Control*, Addison Wesley, Reading, MA, 1989.

APPENDIX A

The body-fixed barycentric vectors are given by [11, 14]

$$\mathbf{v}_{ki}^{(m)} = \begin{cases} \tilde{\mathbf{r}}_k^{(m)} = \mathbf{r}_i^{(m)} - \mathbf{e}_k^{(m)} & k < i \\ \tilde{\mathbf{e}}_k^{(m)} = -\mathbf{e}_k^{(m)} & k = i \\ \tilde{\mathbf{l}}_k^{(m)} = \mathbf{l}_i^{(m)} - \mathbf{e}_k^{(m)} & k > i \end{cases} \quad \begin{cases} m = 1,\ldots,n \\ i = 1,\ldots,N_m \end{cases} \tag{A1}$$

where vectors $\mathbf{r}_i^{(m)}$ and $\mathbf{l}_i^{(m)}$ are defined in Fig. 1, and $\mathbf{e}_i^{(m)}$ are given by

$$\mathbf{e}_i^{(m)} = \mathbf{l}_i^{(m)}(1-\mu_i^{(m)}) + \mathbf{r}_i^{(m)}\mu_{i+1}^{(m)} \tag{A2}$$

$$\mathbf{e}_0 = \sum_{m=1}^{n} \mathbf{r}_0^{(m)}\mu_1^{(m)} \tag{A3}$$

The quantity $\mu_i^{(m)}$ is the outboard mass after joint i in manipulator m, and is given by

$$\mu_i^{(m)} = \sum_{k=i}^{N_m} \frac{m_k^{(m)}}{M} \qquad i = 1,\ldots,N_m \quad \textit{and} \quad \mu_{N_m+1}^{(m)} = 0 \tag{A4}$$

Finally, M is the total mass of the system, and $m_k^{(m)}$ is the mass of the k-th body of the m-th manipulator.

APPENDIX B

The auxiliary control $\mathbf{u}_\omega$ computed according to Eq. (34), is repeated here for completeness

$$\mathbf{u}_\omega = \mathbf{R}_e\dot{\boldsymbol{\omega}}_{des} + \boldsymbol{\omega}^\times\boldsymbol{\omega}_e - \mathbf{K}_v\boldsymbol{\omega}_e - 2(\mathbf{K}_p - \boldsymbol{\omega}_e^T\boldsymbol{\omega}_e/4)\boldsymbol{\varepsilon}_e/n_e \tag{B1}$$

The matrix $\mathbf{R}_e$ is a rotation matrix expressing the error between the desired and current attitude and is defined as

$$\mathbf{R}_e = \mathbf{R}\mathbf{R}_{des}^T \tag{B2}$$

The matrix $\mathbf{R}$ is the rotation matrix which corresponds to the orientation of a body with respect to the inertial frame, and $\mathbf{R}_{des}$ corresponds to the desired orientation. Similarly, the angular velocity $\boldsymbol{\omega}_e$ is the error in angular velocities, expressed in the body-fixed frame

$$\boldsymbol{\omega}_e = \boldsymbol{\omega} - \mathbf{R}_e\boldsymbol{\omega}_{des} \tag{B3}$$

where $\boldsymbol{\omega}$ is the body angular velocity and $\boldsymbol{\omega}_{des}$ the desired one, expressed in the desired orientation frame. Finally, $\boldsymbol{\varepsilon}_e$ and n_e correspond to the error in attitude as expressed by Euler parameters

$$\boldsymbol{\varepsilon}_e = \mathbf{T}_{des}^T\boldsymbol{\varepsilon} - \boldsymbol{\varepsilon}_{des}n \tag{B4}$$

$$n_e = \boldsymbol{\varepsilon}_{des}^T\boldsymbol{\varepsilon} + n_{des}n \tag{B5}$$

with

$$\mathbf{T} = n\mathbf{I} + \boldsymbol{\varepsilon}^\times \tag{B6}$$

where $\mathbf{I}$ is a 3×3 unit matrix, and n and $\boldsymbol{\varepsilon}$ are the current Euler parameters [17].

As shown in [16], applying the control law given by Eq. (34), the attitude error is governed by an homogeneous linear second order differential equation, which guarantees that the error will converge to zero asymptotically

$$\ddot{\boldsymbol{\varepsilon}}_e + \mathbf{K}_d\dot{\boldsymbol{\varepsilon}}_e + \mathbf{K}_p\boldsymbol{\varepsilon}_e = \mathbf{0} \tag{B7}$$